



**HAL**  
open science

# Viscoelastic formulation for modelling of plate tectonics

Louis Moresi, Frédéric Dufour, Hans Mühlhaus

► **To cite this version:**

Louis Moresi, Frédéric Dufour, Hans Mühlhaus. Viscoelastic formulation for modelling of plate tectonics. Bifurcation and Localisation Theory in Geomechanics, 2001, Perth, Australia. 10.1201/9781003210931-46 . hal-01009106

**HAL Id: hal-01009106**

**<https://hal.science/hal-01009106v1>**

Submitted on 19 May 2023

**HAL** is a multi-disciplinary open access archive for the deposit and dissemination of scientific research documents, whether they are published or not. The documents may come from teaching and research institutions in France or abroad, or from public or private research centers.

L'archive ouverte pluridisciplinaire **HAL**, est destinée au dépôt et à la diffusion de documents scientifiques de niveau recherche, publiés ou non, émanant des établissements d'enseignement et de recherche français ou étrangers, des laboratoires publics ou privés.



Distributed under a Creative Commons Attribution 4.0 International License

# Viscoelastic formulation for modeling of plate tectonics.

Louis Moresi, Frédéric Dufour, Hans Mühlhaus  
*CSIRO Exploration and Mining, Perth, 6009, AUSTRALIA*

**ABSTRACT:** The Earth's tectonic plates are strong, viscoelastic shells which make up the outermost part of a thermally convecting, predominantly viscous layer. In order to build a more realistic simulation of the planet's evolution, the complete viscoelastic convection system must be included. A particle-in-cell finite element method is demonstrated which can simulate very large deformation viscoelasticity. This is applied to a plate-deformation problem. Numerical accuracy is demonstrated relative to analytic benchmarks, and the characteristics of the method are discussed.

## 1 INTRODUCTION

Underneath the lithospheric plates of the Earth lies the mantle (Figure 1). Approximately 3000km deep, it is composed of solid rock that is warm enough to deform like a viscous fluid, albeit at incredibly slow speeds of a few centimetres per year. The plates move because the mantle is forever stirring as heat generated by natural radioactive decay struggles to escape via thermal convection. The plates which form the ocean floors are part of this circulation and are sucked down when they become old, cold and dense. The continental crust is formed by lower density rock which remains buoyant despite being cold. In the lithosphere the rocks are significantly cooler and behave as a viscoelastic, brittle solid. In regions of high stress, brittle failure gives rise to earthquakes.

This picture of the Earth's interior is widely accepted by geophysicists. It clearly indicates that the fundamental process is thermal convection; plate tectonics is the manner in which the system organizes. Therefore, a consistent model of plate behaviour must contain a description of the convection system of which the plate is a part.

There are some fundamental problems which need to be addressed before the routine application of engineering principles to the lithosphere. The principle issues is that plate tectonics is itself only a kinematic description of the observations: a fully consistent dynamic description of the motion of the plates is still sought.

There have been some major steps towards the simulation of plate tectonics in recent years by solving brittle/viscous fluid flow equations (e.g. Tackley 1998, 2000, Moresi & Solomatov, 1998). However, incorporating these developments into an engineering description of the lithosphere has proved to be difficult because of the absence of elastic stresses from the simulations. In the past, viscoelastic con-

vection simulations have been limited to models with explicit layering in which a non-convecting viscoelastic layer is coupled to a viscous convecting domain (Podladchikov et al, 1993). Models of subduction zones which incorporate viscoelasticity, faulting, and free-surface behaviour have generally been limited to modest evolution times, after which further deformation produces severe remeshing problems (e.g. Melosh, 1978, Gurnis et al, 1996). The Natural Element Method of Braun & Sambridge (1995) is capable of handling very large deformation viscoelasticity, but with considerable complexity, particularly in the extension to 3D. Having identified the need for efficient, large-scale convection simulations with elastic effects in an evolving cool lithosphere, we present a method for simulating viscoelastic-brittle materials in extreme deformation.

## 2 MATHEMATICAL MODEL

We begin our analysis in a general way with the classical momentum conservation equation:

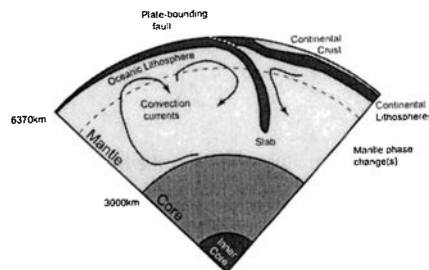


Figure 1: A simplified cross section of the Earth with major layerings shown to scale except for the upper boundary layer which is exaggerated in thickness by a factor of roughly two.

$$\nabla \cdot \boldsymbol{\sigma} = \mathbf{f} \quad (1)$$

where  $\boldsymbol{\sigma}$  is the stress tensor and  $\mathbf{f}$  a force term. As we are interested only in very slow deformations of highly viscous materials, (infinite Prandtl number) we have neglected all inertial terms in (1). It is convenient to split the stress into a deviatoric part,  $\boldsymbol{\tau}$ , and an isotropic pressure,  $p$ ,

$$\boldsymbol{\sigma} = \boldsymbol{\tau} - p\mathbf{I} \quad (2)$$

where  $\mathbf{I}$  is the identity tensor.

### 2.1 Viscoelasticity

There are a number of different viscoelastic models, we will use the Maxwell model which has been used in previous studies of lithospheric deformation where viscous and elastic effects are important such as post-glacial rebound (Peltier, 1974). This model assumes that the strain rate tensor,  $\mathbf{D}$ , defined as:

$$D_{ij} = \frac{1}{2} \left( \frac{\partial V_i}{\partial x_j} + \frac{\partial V_j}{\partial x_i} \right) \quad (3)$$

is the sum of an elastic strain rate tensor  $\mathbf{D}_e$  and a viscous strain rate tensor  $\mathbf{D}_v$ . The velocity vector,  $\mathbf{V}$ , is the fundamental unknown of our problem and all these entities are expressed in the fixed reference frame  $x_i$ . Now we decompose each strain rate tensor

$$\mathbf{D}_e = \frac{1}{3} \text{tr}(\mathbf{D}_e) \mathbf{I} + \hat{\mathbf{D}}_e \quad (4)$$

and

$$\mathbf{D}_v = \frac{1}{3} \text{tr}(\mathbf{D}_v) \mathbf{I} + \hat{\mathbf{D}}_v \quad (5)$$

where  $\hat{\mathbf{D}}$  is the deviatoric part of  $\mathbf{D}$  and  $\text{tr}(\mathbf{D})$  represents the trace of the tensor.

Individually we express each deformation tensor as a function of the deviatoric stress tensor  $\boldsymbol{\tau}$  and pressure  $P$ , which finally gives a tensorial equation:

$$\frac{\overset{\vee}{\boldsymbol{\tau}}}{2\mu} + \frac{\boldsymbol{\tau}}{2\eta} = \hat{\mathbf{D}}_e + \hat{\mathbf{D}}_v = \hat{\mathbf{D}} \quad (6)$$

where  $\overset{\vee}{\boldsymbol{\tau}}$  is the Jaumann corotational stress rate for an element of the continuum,  $\mu$  is the shear modulus and  $\eta$  is shear viscosity. The isotropic part gives a scalar equation for the pressure:

$$\frac{\dot{p}}{K_e} + \frac{p}{\xi} = -\text{tr}(\mathbf{D}) \quad (7)$$

where  $K_e$  is the bulk modulus and  $\xi$  is the bulk viscosity.  $\overset{\vee}{p} \equiv \dot{p}$  as it  $p$  is a scalar.

$$\overset{\vee}{\boldsymbol{\tau}} = \dot{\boldsymbol{\tau}} + \boldsymbol{\tau} \mathbf{W} - \mathbf{W} \boldsymbol{\tau} \quad (8)$$

where  $\mathbf{W}$  is the material spin tensor,

$$W_{ij} = \frac{1}{2} \left( \frac{\partial V_i}{\partial x_j} - \frac{\partial V_j}{\partial x_i} \right) \quad (9)$$

The  $\mathbf{W}$  terms account for material spin during advection which reorients the elastic stored-stress tensor.

We note that the form of equation (7) is unsuited to conventional fluids as the material has no long term resistance to compression. This behaviour is, however, relevant to the simulation of the coupled porous-flow, matrix deformation problem. Here it is common to ascribe an apparent bulk viscosity to the matrix material in order to model compaction effects (e.g. McKenzie 1984), particularly for large scale geological systems where the details of the pore network cannot be measured directly.

### 2.2 Numerical implementation

As we are interested in solutions where very large deformations may occur — including thermally driven fluid convection, we would like to work with a fluid-like system of equations. Hence we obtain a stress / strain-rate relation from (6) by expressing the Jaumann stress-rate in a difference form:

$$\overset{\vee}{\boldsymbol{\tau}} \approx \frac{\boldsymbol{\tau}^{t+\Delta t} - \boldsymbol{\tau}^t}{\Delta t} - \mathbf{W}^t \boldsymbol{\tau}^t + \boldsymbol{\tau}^t \mathbf{W}^t \quad (10)$$

where the superscripts  $t, t + \Delta t$  indicate values at the current and future timestep respectively. (6) and (7) become respectively

$$\begin{aligned} \boldsymbol{\tau}^{t+\Delta t} = & \frac{\eta \Delta t}{\alpha + \Delta t} \hat{\mathbf{D}}^{t+\Delta t} + \frac{\alpha}{\alpha + \Delta t} \boldsymbol{\tau}^t \\ & + \frac{\alpha \Delta t}{\Delta t + \alpha} (\mathbf{W}^t \boldsymbol{\tau}^t - \boldsymbol{\tau}^t \mathbf{W}^t) \end{aligned} \quad (11)$$

and

$$p^{t+\Delta t} = -\frac{\xi \Delta t}{\beta + \Delta t} D_{kk}^{t+\Delta t} + \frac{\beta}{\beta + \Delta t} p^t \quad (12)$$

where  $\alpha = \eta/\mu$  is the shear relaxation time and  $\beta = \xi/K_e$  is the bulk relaxation time. We can simplify the above equations by defining an effective viscosity  $\eta_{\text{eff}}$  and an effective compressibility  $\xi_{\text{eff}}$ :

$$\eta_{\text{eff}} = \eta \frac{\Delta t}{\Delta t + \alpha} \quad \text{and} \quad \xi_{\text{eff}} = \xi \frac{\Delta t}{\Delta t + \beta} \quad (13)$$

Then the deviatoric stress is given by

$$\begin{aligned} \boldsymbol{\tau}^{t+\Delta t} = & \\ \eta_{\text{eff}} \left( \hat{\mathbf{D}}^{t+\Delta t} + \frac{\boldsymbol{\tau}^t}{\mu \Delta t} + \frac{\mathbf{W}^t \boldsymbol{\tau}^t}{\mu} - \frac{\boldsymbol{\tau}^t \mathbf{W}^t}{\mu} \right) \end{aligned} \quad (14)$$

and the pressure by

$$p^{t+\Delta t} = -\xi_{\text{eff}} \left( D_{kk}^{t+\Delta t} - \frac{p^t}{\Delta t K_e} \right) \quad (15)$$

To model an incompressible material  $K_e$  and  $\xi$  are made very large such that  $D_{kk} \approx 0$ .

Our system of equations is thus composed of a quasi-Newtonian viscous part with modified mate-

rial parameters and a right-hand-side term depending on values from the previous timestep. This approach minimizes the modification to the viscous flow code. Instead of using physical parameters for viscosity and bulk modulus, we use effective material properties (13) to take into account elasticity. Then during computations for the force term, we add elastic internal stresses from the previous timestep or from initial conditions.

$$F_i^{e,t} = \frac{\xi^{\text{eff}}}{K_e \Delta t} p_{,i}^{t-\Delta t} - \frac{\eta^{\text{eff}}}{\mu \Delta t} \sigma_{ij,j}^{t-\Delta t} \quad (16)$$

We solve (15) and (14) and obtain a solution for  $D^{t+\Delta t}$ . From this solution we compute the new stress state due to the velocity field and previous stored stresses.

### 2.3 Stability

The approach outlined above is unconditionally stable only if the timestep is larger than the relaxation time for the material, i.e.

$$\Delta t < \frac{\eta}{\mu} \quad (17)$$

in the case of the shear moduli. Alternatively, this means a Deborah number,  $De < 1$ , indicating that the method is appropriate to the viscous, rather than the elastic, limit.

One difficulty is that the timestep is not necessarily chosen to match the physical problem, but by the Courant condition for the chosen mesh. This means that a convergence demonstration for arbitrarily small elements may not be possible for the general case. We are currently addressing this issue.

In practice, however, for our area of research, viscous flow drives the plate motions, and the lithospheric plates are embedded in a highly viscous material. This may produce a situation where a system-wide relaxation time is more important than the relaxation times of individual materials, since loading and unloading of the elastic materials happens almost exclusively through a low-viscosity medium. Under these circumstances, the relaxation time of an individual layer (such as the lithosphere) may be much larger than the Courant timestep, but stresses are either balanced, or relaxed by driving a flow in one of the viscous materials.

## 3 COMPUTATIONAL METHOD

### 3.1 Choice of Numerical Scheme

In fluid dynamics, where strains are generally very large, but not important in the constitutive relationship of the material, it is common to transform the equations to an Eulerian mesh and deal with convective terms explicitly. Problems arise whenever advection becomes strongly dominant over diffusion since an erroneous numerical diffusion dominates. In our case, the advection of material boundaries and the stress tensor are particularly susceptible to this numerical diffusion problem. Mesh-based Lagrangian formulations alleviate this difficulty, but at the expense of remeshing and the eventual development of a

less-than optimal mesh configuration. This increases complexity and can hinder highly efficient solution methods such as multigrid iteration. The Natural Element Method eliminates remeshing difficulties but is associated with considerable complexity of implementation, particularly in 3D.

A number of alternatives are available which dispense with a mesh entirely: smooth particle hydrodynamics and discrete element methods are common examples from the fluid and solid mechanics fields respectively. These methods are extremely good at simulating the detailed behaviour of highly deforming materials with complicated geometries (e.g. free surfaces, fracture development), and highly dynamic systems. They are, in general, formulated to calculate explicitly the interactions between individual particles which ultimately means that a great many timesteps would be required to study creeping flow where the timescales associated with inertial effects are very many orders of magnitude smaller than typical flow times.

We have therefore developed a hybrid approach – a particle in cell finite element method which uses a standard Eulerian finite element mesh (for fast, implicit solution) and a Lagrangian particle framework for carrying details of interfaces, the stress history etc.

### 3.2 The Particle in Cell Approach

Our particle-in-cell finite element method is based closely on the standard finite element method, and is a direct development of the material point method of Sulsky et al. (1995). The standard mesh is used to discretize the domain into elements, and the shape functions interpolate node points in the mesh in the usual fashion. The problem is formulated in a weak form to give an integral equation, and the shape function expansion produces a discrete (matrix) equation. Equation (1) in weak form, using the notation of (2) becomes

$$\int_{\Omega} N_{(i,j)} \tau_{ij} d\Omega - \int_{\Omega} N_{,i} p d\Omega = \int_{\Omega} N_i f_i d\Omega \quad (18)$$

where the trial functions,  $N$ , are the shape functions defined by the mesh, and we have assumed no non-zero traction boundary conditions are present. For the discretized problem, these integrals occur over subdomains (elements) and are calculated by summation over a finite number of sample points within each element. For example, in order to integrate a quantity,  $\phi$  over the element domain  $\Omega^e$  we replace the continuous integral by a summation

$$\int_{\Omega^e} \phi d\Omega \leftarrow \sum_p w_p \phi(\mathbf{x}_p) \quad (19)$$

In standard finite elements, the positions of the sample points,  $\mathbf{x}_p$ , and the weighting,  $w_p$  are optimized in advance. In our scheme, the  $\mathbf{x}_p$ 's correspond precisely to the Lagrangian points embedded in the fluid, and  $w_p$  must be recalculated at the end of a timestep for the new configuration of particles. Constraints on the values of  $w_p$  come from the need to integrate polynomials of a minimum degree related to the degree of the shape function interpolation, and the order of the

underlying differential equation (e.g Hughes, 1987). These Lagrangian points carry the history variables which are therefore directly available for the element integrals without the need to interpolate from nodal points to fixed integration points. In our case, the distribution of particles is usually not ideal, and a unique solution for  $w_p$  cannot be found, or we may find we have negative weights which are not suitable for integrating physical history variables. We therefore store an initial set of  $w_p$ 's based on a measure of local volume and adjust the weights slightly to improve the integration scheme.

Moresi et al. (2000) give a full discussion of the implementation of the particle-in-cell finite element scheme used here including full details of the integration scheme and its assumptions. They also discuss the specific modifications to the material point method required to handle a convecting fluid.

#### 4 BENCHMARKS

We have benchmarked our numerical scheme against analytic solutions in order to characterize its strengths and weaknesses, and to quantify the likely level of accuracy we can achieve with a given mesh/particle density. We first benchmark the purely viscous flow case to provide a baseline for comparison with viscoelastic cases.

##### 4.1 Analytical solution

We study the spreading of a rectangular sample of material under a constant downward velocity  $V$  applied on top (see Fig.2).

The specified boundary conditions give:

$$\sigma_{xx} = \tau_{xx} - p = 0 \quad (20)$$

which is substituted into the  $x$  component of (6) to give an expression in the pressure

$$\frac{\dot{p}}{2\mu} + \frac{p}{2\eta} = \frac{1}{2}(D_{xx} - D_{zz}) \quad (21)$$

$D_{xx}$  can be eliminated between (21) and (7), and  $D_{zz}$  is given kinematically as

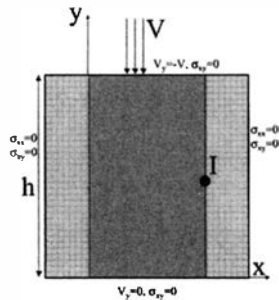


Figure 2: Geometry and boundary conditions for the analytic solution.

$$D_{zz} = -\frac{V}{h_0 - Vt} \quad (22)$$

where  $h_0$  is the initial height. Hence

$$a\dot{p}(t) + bp(t) = -\frac{2V}{h_0 - Vt} \quad (23)$$

with

$$a = -\frac{1}{K_e} - \frac{1}{\mu} \quad \text{and} \quad b = -\frac{1}{\xi} - \frac{1}{\eta} \quad (24)$$

The solution to this equation is

$$p(t) = \frac{2e^{\frac{b}{a}(h_0 - Vt)}}{a} \times \left\{ \ln \left( 1 - \frac{V}{h_0} t \right) + \sum_{i=1}^{\infty} \left( -\frac{b h_0}{a V} \right)^i \frac{(1 - \frac{V}{h_0} t)^i - 1}{i \cdot i!} \right\} \quad (25)$$

We use this relationship to eliminate the pressure derivative from (21) and (7) and express the unknown  $D_{xx}$  as a function of  $p$  and  $D_{zz}$ . Consequently we obtain a relation between the velocity  $V_x$  of a point and its coordinate  $x$ .

$$V_x = -\frac{x}{K_e + \mu} \times \left( p \left( \frac{K_e}{\xi} - \frac{\mu}{\eta} \right) + D_{zz}(K_e - \mu) \right) \quad (26)$$

##### 4.2 Model

The Eulerian mesh does not carry any information from timestep to timestep other than the boundary conditions. Therefore, when convenient, the mesh may be modified, replaced, and refined as necessary. For this problem, compression is applied by a moving boundary condition which causes the mesh to compact in one direction. For simplicity, the mesh is simply scaled to the new aspect ratio without altering the number of elements. In a more complicated situation, however, it would be possible to regrid completely without loss of accuracy. The only detail which needs to be observed is that the updating of the boundary node locations follows the same formulation as that of the particles (here, a second order Runge-Kutta integration procedure) to prevent the boundary conditions from drifting with respect to the stored information on the particles.

In the  $x$ -direction we have a free surface. In order to investigate the properties of a particle representation of such interfaces, it is important not to simply use a mesh-based boundary condition. Instead we use a mesh (Fig. 2) larger than the specimen and fill the gap with a background material having ( $\eta = 10^3$  MPa.s and  $\xi = 10^5$  MPa.s).

The square mesh is composed of 4096 elements.

### 4.3 Results

We have tested the code, ELLIPSIS, with three different type of materials: viscous and compressible Fig.(3.c and d), viscous and incompressible Fig.(3.a and b), viscoelastic and compressible Fig.(4). The numerical parameters for the viscous part of (15) and (14) are:

$$\eta = 10^6 \text{ MPa.s.} \quad \text{and} \quad \xi = 4.10^6 \text{ MPa.s.} \quad (27)$$

Due to the mesh size and the prescribed velocity on top, the Courant condition requires  $\Delta t < 5.10^{-3}$  s.. For our problem we take  $\Delta t = 10^{-3}$  s..

As an indicator of accuracy we compare analytical and numerical x-velocity at the point I (Fig. 2). The steps in the numerical solutions are related to the the motion of the material interface relative to the element edges. When the interface between the specimen and the background material crosses into a new element there is an immediate discontinuous contribution to the element equations from the sample material. We have verified that jump tends to zero as we increase the element and particle densities.

In the viscoelastic case, in Fig. (4) we can see that, for different relaxation time, the error against the analytical solution remains below 3%. Some steps are still present, but in the viscoelastic case the velocity is considerably more noisy. What is most clear is that the computations with larger relaxation time have greater fluctuation in accuracy. The problem becomes more acute in this case when the Courant time (decreasing due to the compression of the background mesh) becomes comparable to the relaxation time. This can result in a loss of stability which is entirely an artefact of the discretization. The most promising solution to this issue is to compute the time-derivative of the stress tensor over a physically relevant interval, rather than that imposed by the mesh. This is a particular focus of our current research.

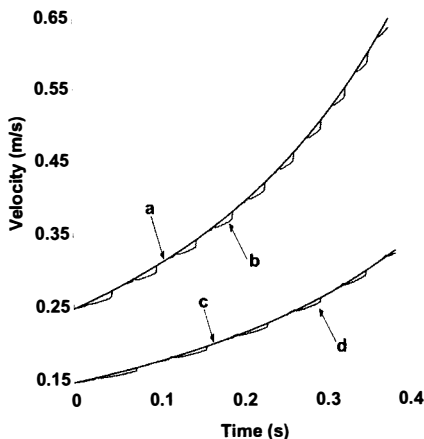


Figure 3: Viscous deformation results: a. viscous incompressible, analytical, b. viscous incompressible, numerical, c. viscous compressible, analytical and d. viscous compressible, numerical.

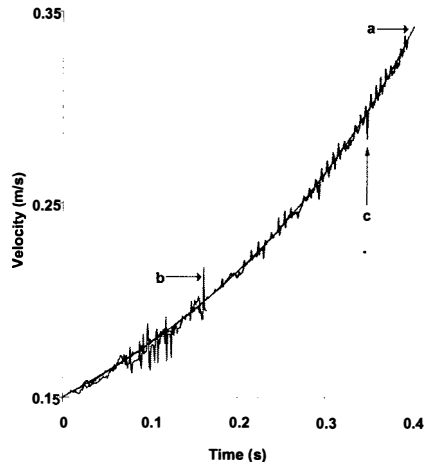


Figure 4: Viscoelastic material a. Numerical solution, b.  $\mu = 10^4$  MPa., c.  $\mu = 10^5$  MPa.

## 5 APPLICATION TO PLATE DYNAMICS

### 5.1 Mathematical Model

We treat the Earth on a large scale as an incompressible, viscoelastic Maxwell fluid with infinite Prandtl number in which motions are driven by internal temperature variations. The force term from equation (1) is a gravitational body force due to density changes. We assume that these arise, for any given material, through temperature effects:

$$\nabla \cdot \boldsymbol{\tau} - \nabla p = g\rho_0(1 - \alpha T)\hat{\mathbf{z}} \quad (28)$$

where  $g$  is the acceleration due to gravity,  $\rho_0$  is material density at a reference temperature,  $\alpha$  is the coefficient of thermal expansivity, and  $T$  is temperature.  $\hat{\mathbf{z}}$  is a unit vector in the vertical direction. We have also assumed that the variation in density only needs to be considered in the driving term (the Boussinesq approximation).

The equation of motion is then

$$\begin{aligned} \nabla(\eta_{\text{eff}}\mathbf{D}^{t+\Delta t}) - \nabla p = g\rho_0(1 - \alpha T)\hat{\mathbf{z}} - \\ \nabla \left( \eta_{\text{eff}} \left[ \frac{\boldsymbol{\tau}^t}{\mu\Delta t} + \frac{\mathbf{W}^t\boldsymbol{\tau}^t}{\mu} - \frac{\boldsymbol{\tau}^t\mathbf{W}^t}{\mu} \right] \right) \end{aligned} \quad (29)$$

The velocity field  $\mathbf{u}$  and pressure at  $t + \Delta t$  can be solved for a given temperature distribution and the stress history from the previous step.

Motion is driven by the heat escaping from the interior. The energy equation governs the evolution of the temperature in response to diffusion of heat through the fluid. For a given element of fluid,

$$\frac{DT}{Dt} = -\kappa\nabla^2 T \quad (30)$$

where  $\kappa$  is the thermal diffusivity of the material.

So far, all equations have been written in a purely

Lagrangian framework. The time derivate of temperature and the Jaumann stress rate refer to a frame of reference which is carried by the fluid. In choosing a solution method, it is necessary to choose whether to honour the Lagrangian formulation, or to work with a fixed reference frame and introduce additional terms to compensate for the advection of temperature and stress by the fluid.

## 5.2 Brittle failure

As we discussed above, plate models need to include a description of the brittle nature of the coldest part of the lithosphere. Geologists use this term quite loosely to distinguish fault-dominated deformation which may result in seismic activity, from ductile creep which occurs at higher temperature and pressure. In all recent studies of mantle convection where the brittle lithospheric rheology has been taken into account, the brittle behaviour has been parameterized using a non-linear effective viscosity which is introduced whenever the stress would otherwise exceed the yield value  $\tau_{\text{yield}}$ . This approach ignores details of individual faults, and treats only the influence of fault systems on the large-scale convective flow.

To determine the effective viscosity we extend (6) by introducing a von Mises plastic flow rule:

$$\frac{\dot{\boldsymbol{\tau}}}{2\mu} + \frac{\boldsymbol{\tau}}{2\eta} + \lambda \frac{\boldsymbol{\tau}}{2|\boldsymbol{\tau}|} = \hat{\mathbf{D}}_e + \hat{\mathbf{D}}_v + \hat{\mathbf{D}}_p = \hat{\mathbf{D}} \quad (31)$$

where  $\lambda$  is a parameter to be determined such that the stress remains on the yield surface, and  $|\boldsymbol{\tau}| \equiv (\tau_{ij}\tau_{ij}/2)^{(1/2)}$ . We again express the Jaumann stress rate in difference form (10) to give:

$$\boldsymbol{\tau}^{t+\Delta t} \left[ \frac{1}{2\mu\Delta t} + \frac{1}{2\eta} + \frac{\lambda}{2|\boldsymbol{\tau}|} \right] = \hat{\mathbf{D}}^{t+\Delta t} + \frac{1}{2\mu\Delta t} \boldsymbol{\tau}^t + \frac{1}{2\mu} (\mathbf{W}^t \boldsymbol{\tau}^t - \boldsymbol{\tau}^t \mathbf{W}^t) \quad (32)$$

No modification to the isotropic part of the problem is required when the von Mises yield criterion is used. At yield we use the fact that  $|\boldsymbol{\tau}| = \tau_{\text{yield}}$  to write

$$\boldsymbol{\tau}^{t+\Delta t} = \eta' \left[ 2\hat{\mathbf{D}}^{t+\Delta t} + \frac{1}{\mu\Delta t} \boldsymbol{\tau}^t + \frac{1}{\mu} (\mathbf{W}^t \boldsymbol{\tau}^t - \boldsymbol{\tau}^t \mathbf{W}^t) \right] \quad (33)$$

using an effective viscosity,  $\eta'$  given by

$$\eta' = \frac{\eta\tau_{\text{yield}}\mu\Delta t}{\eta\tau_{\text{yield}} + \tau_{\text{yield}}\mu\Delta t + \lambda\eta\mu\Delta t} \quad (34)$$

We determine  $\lambda$  by equating the value of  $|\boldsymbol{\tau}^{t+\Delta t}|$  with the yield stress in (33). Alternatively, in this particular case, we can obtain  $\eta'$  directly as

$$\eta' = \tau_{\text{yield}} / |\hat{\mathbf{D}}_{\text{eff}}| \quad (35)$$

where

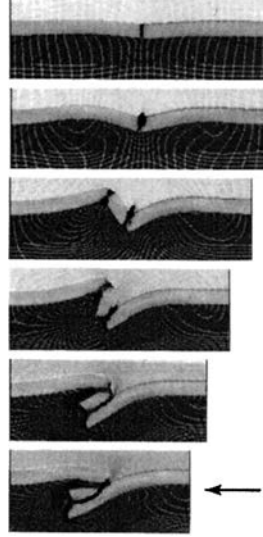


Figure 5: Example: compression of a viscoelastic plate with yield stress overlying a low viscosity fluid of equal density

$$\hat{\mathbf{D}}_{\text{eff}} = 2\hat{\mathbf{D}}^{t+\Delta t} + \frac{1}{\mu\Delta t} \boldsymbol{\tau}^t + \frac{1}{\mu} (\mathbf{W}^t \boldsymbol{\tau}^t - \boldsymbol{\tau}^t \mathbf{W}^t) \quad (36)$$

and  $|\mathbf{D}| = (2D_{ij}D_{ij})^{1/2}$ .

The value of  $\lambda$  or  $\eta'$  is iterated to allow stress to redistribute from particles which become unloaded. The iteration is repeated until the velocity solution is unchanged to within the error tolerance required for the solution as a whole.

The value of the yield stress is, in principle, a function of strain, yield history, and temperature, and can be distinct for different materials.

## 6 PLATE MODELING

As a simple example, we demonstrate the compression of a viscoelastic-brittle layer which lies on top of a slightly less dense viscous fluid layer (Figure 5). This system is an analogue of the cool oceanic lithosphere which rests upon the warm asthenosphere (though we do not solve the temperature equation in this case). The viscoelastic layer is initially split to provide an initiation point for a model subduction zone. The vertical boundaries are free-slip, and the right hand edge is given a horizontal velocity to shorten the system. There is a layer of highly compressible material of very low viscosity above the elastic layer which accomodates the volume change associated with shortening of the mesh, and mimics a free surface boundary condition on the upper surface of the elastic layer. As compression proceeds, the viscoelastic layer flexes and the viscous layer flows to accomodate the deformation. As stresses build up in the model lithosphere, a second failure point develops allowing one half of the material to fold up under the other half. Further compression forces the two halves of the lithosphere layer to slide past each other along a zone of material failure. After this point, the pres-

ence of the bottom boundary begins to interfere with the evolution of the system.

This particular simulation demonstrates the capability of the algorithm in the simulation of subduction zone geometry in the style of Melosh (1978) or Gurnis et al. (1996). The fact that the algorithm is implemented within a fluid-dynamics framework suggests that a viscoelastic analysis of convection with strong temperature dependence of viscosity and a yield stress is now possible.

## 7 DISCUSSION

The algorithm described above is designed to introduce elastic effects into convection simulations where temperature-dependent viscosity and yielding dominate the mechanical behaviour. The viscosity of the mantle and the mantle lithosphere is very strongly dependent on temperature (several orders of magnitude variation over 1000°C) whereas the shear modulus is not strongly affected (there is only a modest change in seismic wavespeed due to temperature). Therefore, elastic effects become unimportant outside the cold thermal boundary layer where viscosity is extremely large.

The influence of elastic stresses is likely to be felt at the subduction zones where the lithosphere is bent into the interior of the Earth. In these regions stresses are typically close to the yield stress — a fact which allows the plates to move in the first place. The addition of elasticity is likely to complicate the simple picture presented by Tackley (1998) and Moresi & Solomatov (1998) for viscous materials with a yield stress.

Our methodology is limited to a coarse continuum description of the subduction zone system at a resolution of a few km. This may be able to give us valuable information into the nature of plate tectonics, the thermal conditions in and around subducting lithosphere, and the stress state of the system. However, the resolution is too coarse to say anything about the detailed mechanics of the failure of lithospheric fault zones and the conditions for major failure to occur. For this we require a coupling of the large-scale code with an engineering-scale code (e.g. DEM or small-deformation Lagrangian FEM) using the large-scale to provide boundary conditions for the small scale. The issue of scale-bridging is important in many areas of numerical simulation. Essentially the same difficulties arise in material science where the atomic scale is best treated by molecular dynamics codes but the large scale must be treated as a continuum (e.g. Bernholc, 1999).

## ACKNOWLEDGEMENTS

The authors gratefully acknowledge the suggestions of an anonymous reviewer which have helped to clarify this paper.

## REFERENCES

Bernholc, J., 1999, Computational materials science: The era of applied quantum mechanics, *Physics Today*, 52, No 9, 30–35.

Braun, J., Sambridge, M., 1995, A numerical method for solving partial differential equations on highly irregular evolving grids, *Nature*, 376, 655–660.

Gurnis, M., Eloy, C., Zhong, S., 1996, Free-surface formulation of mantle convection — II. Implications for subduction zone observables, *Geophys. J. Int.*, 127, 719–727.

Hughes, T. J.R., 1984, *The Finite Element Method*, Prentice-Hall.

Melosh, H. J., 1978, Dynamic support of the outer rise, *Geophys. Res. Lett.*, 5, 321–324.

Moresi, L., Mühlhaus, H.-B., Dufour, F., Proceedings of the 5th International Workshop on Bifurcation and Localization in Geomechanics, Perth, W. A., Australia, Balkema.

Moresi, L., Solomatov, V. S., 1998, Mantle convection with a brittle lithosphere: thoughts on the global tectonics styles of the Earth and Venus, *Geophys. J. Int.*, 133, 669–682.

McKenzie, D., 1984, The generation and compaction of partially molten rock, *J. Petrology*, 25, 713–765.

Peltier, W. R., 1974, The impulse response of a Maxwell Earth, *Rev. Geophys. Space Phys.* 12, 649–669.

Podlachikov, Yu., Yu., Lenardic, A., Yuen, D. A., Quareni, F., 1993, Dynamical consequences of stress focussing for different rheologies: Earth and Venus perspectives, *EOS Trans. AGU*, 74 no. 43/Suppl., 566.

Sulsky, D., Zhou, S.-J., Schreyer, H. L., 1995, Application of a particle-in-cell method to solid mechanics, *Comput. Phys. Commun.* 87, 236–252.

Tackley, P. J., 1998, Self-consistent generation of tectonic plates in three dimensional mantle convection, *Earth Planet. Sci. Lett.*, 157, 9–22.

Tackley, P. J., 2000, The quest for self-consistent generation of plate tectonics in mantle convection models, *AGU Monograph on The history and dynamics of global plate motions*, ed. M. Richards, In Press.